European Journal of Clinical and Biomedical Sciences
2026; 12(3): 54-61
http://www.sciencepublishinggroup.com/j/ejcbs
doi: 10.11648/j.ejcbs.20261203.12

AMAtt: Manifold Attention Network with Adaptive Log-Euclidean Metrics for Brain Signals

Syed Mohamed Syed Abubakar Shaihan[1, 2, 3, *]

[1]Department of Computer Science, Control and Management, Sapienza University of Rome, Rome, Italy
[2]Department of Mechanical Engineering, Indian Institute of Science, Bangalore, India
[3]Department of Electronics and Communication Engineering, Anjuman Institute of Technology and Management, Bhatkal, India

Email address:

smshaihan@gmail.com (Syed Mohamed Syed Abubakar Shaihan)

To cite this article:

Syed Mohamed Syed Abubakar Shaihan. (2026). AMAtt: Manifold Attention Network with Adaptive Log-Euclidean Metrics for Brain Signals. *European Journal of Clinical and Biomedical Sciences, 12*(3), 54-61. https://doi.org/10.11648/j.ejcbs.20261203.12

Received: 5 April 2026; **Accepted:** 20 April 2026 **Published:** 27 August 2026

Abstract: In this paper, we discuss the recognition of electroencephalographic (EEG) signals, which is crucial in order to improve the performance of non-invasive brain-computer interfaces (BCIs). Although deep learning (DL) has achieved considerable advancements in the decoding of EEG signals, it frequently encounters difficulties related to noisy data and non-stationarity challenges. We discuss geometric learning which offers a more robust way to handle EEG signals by leveraging the mathematical structure of the data. We extended the existing Manifold Attention Network (MAtt), a novel deep learning model that applies a manifold attention mechanism to better capture the spatiotemporal patterns of EEG signals. Instead of using traditional Euclidean space, we mapped the data onto a Riemannian symmetric positive definite (SPD) manifold, which allows for more effective feature extraction. One major issue with existing SPD-based deep learning approaches is that they rely on fixed Riemannian metrics, which can be suboptimal. To solve this, we integrate Adaptive Log-Euclidean Metrics (ALEMs)—a learnable metric framework into the MAtt network that adapts to the specific structure of EEG data, improving model performance with minimal extra computation. AMAtt achieves 63.19% accuracy on BCIC-IV-2a and 46.00% on MAMEM-SSVEP-II, outperforming the MAtt baseline by 5.55% and 4.60% respectively. This adaptive geometric approach opens new possibilities for robust, subject-independent EEG decoding, paving the way towards practical BCI systems.

Keywords: EEG, Manifold Attention Network, Adaptive Log-Euclidean, SPD, BCI

1. Introduction

Brain-Computer Interfaces (BCIs) have emerged as a revolutionary technology for enabling direct communication between the human brain and external devices. By leveraging neural signals, BCIs offer a pathway for controlling applications such as prosthetic devices and communication aids for individuals with disabilities specially people with paralysis and similar problems [2, 3]. Electroencephalography (EEG) is one of the most widely used modalities in BCI research due to its non-invasive nature, affordability, and portability. EEG-based BCIs have been employed in various real-world applications, such as motor-imagery (MI) BCI-controlled rehabilitation for stroke patients and steady-state visual evoked potential (SSVEP)-based typing systems for individuals with motor impairments [4, 5]. However, despite its advantages, EEG signals are highly susceptible to noise, non-stationarity, and individual variability, making accurate and robust decoding a persistent challenge.

Convolutional Neural Networks (CNNs), in particular, have demonstrated great results in capturing spatial and temporal patterns in EEG data. These networks employ specialized convolutional kernels that act as adaptive spatial and temporal filters, enhancing the model's ability to extract meaningful features. While CNNs and other DL-based models have improved EEG decoding accuracy, they often struggle with the low signal-to-noise ratio (SNR) and dynamic variations in EEG signals.

To address these limitations, geometric learning (GL) has been introduced in BCI research, offering a promising approach to EEG decoding by incorporating Riemannian geometry (RG). RG provides a structured mathematical framework for analyzing EEG covariance matrices on the Symmetric Positive Definite (SPD) manifold. Unlike Euclidean approaches, RG-based methods can better preserve the relationships between data points, making them more robust to outliers and non-stationary signal variations. Classical RG-based EEG decoding methods, such as the Minimum Distance to Mean (MDM) classifier and Tangent Space Linear Discriminant Analysis (TSLDA) [6], have demonstrated their effectiveness in various BCI competitions. However, these methods still rely on manually crafted features and lack the flexibility of deep learning models.

Geometric Deep Learning (GDL) has recently gained traction as an approach that combines the power of deep neural networks with non-Euclidean structures such as graphs and manifolds [7]. GDL enables the direct integration of Riemannian geometry into deep learning models, leading to more robust and generalizable EEG decoding frameworks. Existing GDL methods for EEG decoding have attempted to merge Euclidean-based and manifold-based modules to leverage both spatial and temporal features. However, many of these approaches either fail to fully exploit the temporal information of EEG signals on the manifold or still rely on Euclidean transformations, limiting their effectiveness.

In this work, we build upon recent advancements in GDL and propose an improved EEG decoding framework by integrating adaptive Riemannian metrics into deep learning models. Specifically, we implement the Manifold Attention Network (MAtt) from prior work [1], which is designed to map EEG features onto a Riemannian SPD manifold while effectively capturing their spatiotemporal dynamics. However, instead of using the standard Euclidean-to-Riemannian (E2R) layer, we introduce Adaptive Log-Euclidean Metrics (ALEMs) [8] to enhance feature representation on the SPD manifold. ALEMs dynamically adapt to the statistical properties of EEG data, providing an optimized Riemannian metric that improves both classification accuracy and generalization across subjects and datasets. Unlike traditional Riemannian metrics, which are fixed and predefined, ALEM introduces learnable parameters that allow the model to adjust its representation based on the underlying data distribution.

Compared to other recent EEG decoding methods, AMAtt demonstrates competitive performance. EEGNet [15], a compact CNN-based model, typically achieves around 55–60% on the BCIC-IV-2a dataset, while ShallowConvNet [16] achieves approximately 58–62%. Riemannian-based methods such as the MDM classifier and TSLDA [6] have reported accuracies in the range of 60–65% depending on preprocessing and subject selection. Our proposed AMAtt achieves 63.19% on BCIC-IV-2a, which is comparable to or exceeds these approaches while also offering the advantage of adaptive, learnable Riemannian metrics that generalize across different task types (MI and SSVEP).

2. Preliminaries

In this section, we review fundamental concepts of Riemannian geometry and the symmetric positive definite (SPD) manifold, which form the mathematical foundation of our approach.

2.1. Manifolds and Riemannian Geometry

A manifold is a topological space that locally resembles Euclidean space. A differentiable manifold is a manifold equipped with a smooth structure that allows for calculus-based operations. When a differentiable manifold is further endowed with a Riemannian metric, it becomes a Riemannian manifold, enabling the definition of distances and angles.

The SPD manifold, denoted as $\mathrm{Sym}^+(n)$, is the space of all $n \times n$ symmetric positive definite matrices. This manifold plays a crucial role in signal processing and machine learning, particularly for representing covariance matrices of multivariate data, such as EEG signals.

2.2. Log-euclidean Metric and SPD Geometry

The Riemannian structure of the SPD manifold is commonly studied with two primary metrics: the affine-invariant metric (AIM) and the Log-Euclidean metric (LEM). AIM provides a natural geodesic distance but requires computationally expensive iterative solutions for computing the Riemannian mean. Instead, we leverage LEM, which simplifies computations by mapping the SPD manifold to a vector space via the matrix logarithm function. The Log-Euclidean distance between two SPD matrices P_1, P_2 is given by [9, 10]:

$$\delta_L(P_1, P_2) = \| \log(P_1) - \log(P_2) \|_F$$

where $\| \cdot \|_F$ represents the Frobenius norm. The Log-Euclidean mean of a set of SPD matrices $\{P_1, \dots, P_k\}$ is [11]:

$$G = \exp\left(\frac{1}{k} \sum_{l=1}^{k} \log(P_l) \right)$$

This closed-form solution enables efficient computations in deep learning frameworks.

2.3. Notations

We define key mathematical notations used throughout this paper:

1) $\mathrm{Sym}(n)$: Space of $n \times n$ real symmetric matrices.
2) $\mathrm{Sym}^+(n)$: Space of $n \times n$ symmetric positive definite matrices.
3) $\langle A, B \rangle_F = \mathrm{Tr}(A^T B)$: Frobenius inner product.
4) $\log(P)$ and $\exp(S)$: Logarithm and exponential maps of matrices, computed via eigen decomposition.

3. Methodology

In this section, we present the methodology of our proposed framework, which integrates the Adaptive Log-Euclidean Metric (ALEM) into the E2R (Euclidean to Riemannian) layer of the MAtt (Manifold Attention) architecture. The overall architecture consists of four main components: (1) Feature Extraction (FE), (2) E2R Layer with ALEM, (3) Manifold Attention Module, and (4) R2E (Riemannian to Euclidean) Layer. Below, we describe each component in detail.

3.1. Feature Extraction of EEG Signals

We adopt a two-layer convolutional neural network (CNN) to extract spatiotemporal features from raw EEG signals. The first convolutional layer performs spatial filtering on the multi-channel EEG signals, while the second layer extracts spatiotemporal features. The parameter settings for these layers follow the approach described in [1]. Let $\tilde{f}$ denote the feature embeddings obtained from the CNN. These embeddings are then passed to the E2R layer for transformation into the Riemannian space.

3.2. From Euclidean Space to SPD Manifold (E2R Operation with ALEM)

The E2R layer maps the Euclidean feature embeddings $\tilde{f}$ to the Symmetric Positive Definite (SPD) manifold $\mathrm{Sym}^+(n)$. This is achieved by computing the sample covariance matrices (SCMs) of the embeddings. Specifically, we divide the embeddings $\tilde{f}$ into m epochs, denoted as $\tilde{f}_1, \tilde{f}_2, \ldots, \tilde{f}_m$. For each epoch $\tilde{f}_i$, we compute its SCM as follows:

$$\mathrm{SCM}_{\tilde{f}_i} = \tilde{f}_i \tilde{f}_i^T + \epsilon I,$$

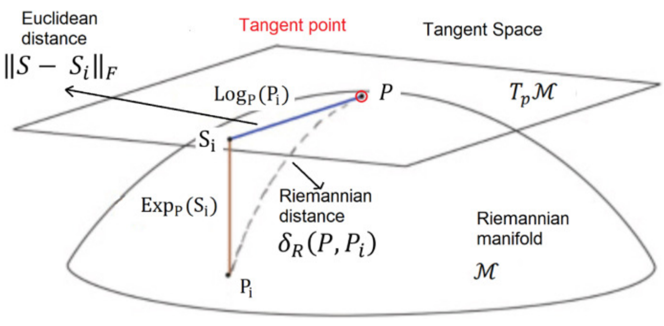

Figure 1. The above figure is the representation of the transformation from Euclidean space to the Riemannian Manifold explained in detail here [14].

where ϵ is a small constant (set to 1×10^{-5} in our implementation) added to ensure positive definiteness, and I is the identity matrix. The resulting sequence of SPD matrices is denoted as $\tilde{X} = [\tilde{x}_1, \tilde{x}_2, \ldots, \tilde{x}_m]$, where each $\tilde{x}_i \in \mathrm{Sym}^+(n)$.

To incorporate the Adaptive Log-Euclidean Metric (ALEM), we generalize the traditional Log-Euclidean Metric (LEM) by introducing a learnable base vector $\alpha = (a_1, a_2, \ldots, a_n) \in \mathbb{R}^n_+ \setminus \{(1, 1, \ldots, 1)\}$. The ALEM is defined as the pullback metric from the Euclidean space $\mathbb{S}^n$ using a generalized matrix logarithm $\mathrm{mlog}(\cdot)$ [8, 12]:

$$\mathrm{mlog}(S) = U \log_\alpha(\Sigma) U^T,$$

where $S = U \Sigma U^T$ is the eigendecomposition of S, and $\log_\alpha(\Sigma) = \mathrm{diag}(\log_{a_1} \sigma_1, \log_{a_2} \sigma_2, \ldots, \log_{a_n} \sigma_n)$ is the diagonal logarithm. The inverse mapping $\mathrm{mlog}^{-1}(\cdot)$ is given by:

$$\mathrm{mlog}^{-1}(X) = U \alpha(\Sigma) U^T,$$

where $\alpha(\Sigma) = \mathrm{diag}(a_1^{\sigma_1}, a_2^{\sigma_2}, \ldots, a_n^{\sigma_n})$. This allows us to define the Adaptive Log-Euclidean Distance (ALED) between two SPD matrices S_1 and S_2 as:

$$\delta_{\mathrm{ALE}}(S_1, S_2) = \|\mathrm{mlog}(S_1) - \mathrm{mlog}(S_2)\|_F,$$

where $\|\cdot\|_F$ is the Frobenius norm. The ALEM provides a flexible and learnable Riemannian metric that adapts to the data distribution.

3.3. Manifold Attention Module

The manifold attention module operates on the sequence of SPD matrices $\tilde{X} = [\tilde{x}_1, \tilde{x}_2, \ldots, \tilde{x}_m]$. The module computes query (q_i), key (k_i), and value (v_i) matrices for each $\tilde{x}_i$ using bilinear mappings:

$$q_i = W_q \tilde{x}_i W_q^T, \quad k_i = W_k \tilde{x}_i W_k^T, \quad v_i = W_v \tilde{x}_i W_v^T,$$

where $W_q, W_k, W_v \in \mathbb{R}^{d_u \times d_c}$ are learnable transformation matrices, and $d_u < d_c$ ensures dimensionality reduction. To ensure that q_i, k_i, v_i remain SPD matrices, W_q, W_k, W_v are constrained to be row-full rank.

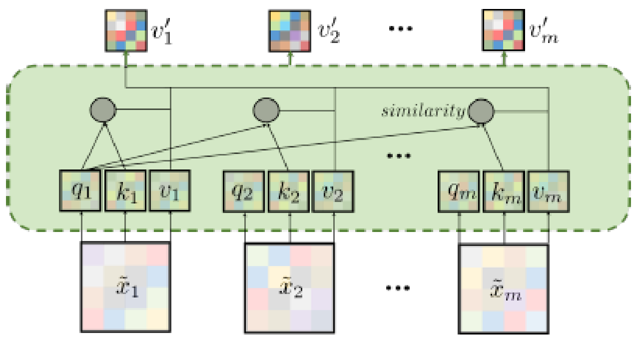

Figure 2. The architecture of the proposed manifold attention module. qi, ki, vi refer to the query, key, and value of the ith input matrix xi respectively; vi stands for the ith output of the proposed module [1].

The similarity between query q_i and key k_j is computed using the ALEM-based distance:

$$\mathrm{sim}(q_i, k_j) = \frac{1}{1 + \log(1 + \delta_{\mathrm{ALE}}(q_i, k_j))} := \alpha_{ij}.$$

The attention matrix $A = [\alpha_{ij}]_{m \times m}$ is then normalized using the Softmax function:

$$A' = \text{Softmax}(A) = \left[\frac{\exp(\alpha_{ij})}{\sum_{k=1}^{m} \exp(\alpha_{ik})} \right]_{m \times m}.$$

The output of the attention module is computed as the Log-Euclidean mean of the value matrices $v_1, v_2, \dots, v_m$ weighted by the attention scores:

$$v_i' = \text{Exp}\left(\sum_{l=1}^{m} \alpha_{il}' \text{Log}(v_l) \right).$$

3.4. From Riemannian Manifold to Euclidean Space (R2E)

After the manifold attention module, the SPD matrices $v_1', v_2', \dots, v_m'$ are mapped back to Euclidean space using the R2E operation. This involves applying the matrix logarithm $\text{Log}(\cdot)$ followed by a flattening operation as shown in [1]:

$$\begin{aligned} h_L(v_i') &= \text{flatten}(\text{Log}(v_i')) \\ &= \text{flatten}(U \text{diag}(\log \sigma_1, \dots, \log \sigma_{d_u}) U^T), \end{aligned}$$

where U and $\sigma_1, \dots, \sigma_{d_u}$ are the eigenvectors and eigenvalues of v_i', respectively. The flattened vectors are then passed through a fully connected layer and a Softmax classifier for final classification.

3.5. Architecture

The proposed architecture consists of four main components: (1) Feature Extraction (FE), (2) E2R Layer with Adaptive Log-Euclidean Metric (ALEM), (3) Manifold Attention Module, and (4) R2E Layer. Each component is designed to process EEG signals in a hierarchical manner, transitioning from Euclidean space to the Riemannian manifold and back to Euclidean space for final classification. below we describe each component in detail.

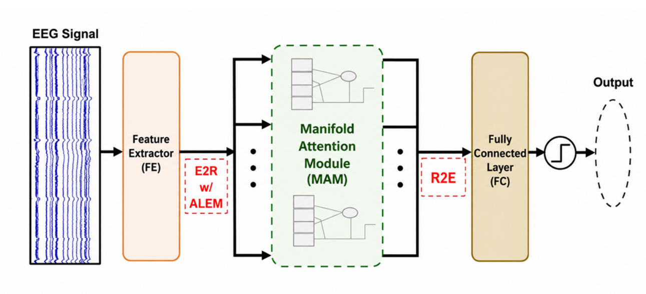

Figure 3. The overview of the proposed model AMAtt archi-tecture.

The feature extraction module is responsible for extracting spatiotemporal features from raw EEG signals. We employ a two-layer convolutional neural network (CNN) for this purpose. The first convolutional layer performs spatial filtering on the multi-channel EEG signals, while the second layer extracts spatiotemporal features. Let $\mathbf{X} \in \mathbb{R}^{C \times T}$ denote the raw EEG signal, where C is the number of channels and T is the number of time samples. The feature extraction process can be described as:

$$\tilde{f} = \text{CNN}(\mathbf{X}),$$

where $\tilde{f} \in \mathbb{R}^{d_c \times T'}$ represents the extracted feature embeddings, d_c is the number of feature channels, and T' is the reduced time dimension after convolution. These embeddings are then passed to the E2R layer for transformation into the Riemannian space.

The E2R layer maps the Euclidean feature embeddings $\tilde{f}$ to the Symmetric Positive Definite (SPD) manifold $\text{Sym}^+(n)$. This is achieved by computing the sample covariance matrices (SCMs) of the embeddings. Specifically, we divide the embeddings $\tilde{f}$ into m epochs, denoted as $\tilde{f}_1, \tilde{f}_2, \dots, \tilde{f}_m$. For each epoch $\tilde{f}_i$, we compute its SCM.
where ϵ is a small constant (set to 1×10^{-5} in our implementation) added to ensure positive definiteness, and I is the identity matrix. The resulting sequence of SPD matrices is denoted as $\tilde{X} = [\tilde{x}_1, \tilde{x}_2, \dots, \tilde{x}_m]$, where each $\tilde{x}_i \in \text{Sym}^+(n)$.

To incorporate the Adaptive Log-Euclidean Metric (ALEM) , we generalize the traditional Log-Euclidean Metric (LEM) by introducing a learnable base vector $\alpha = (a_1, a_2, \dots, a_n) \in \mathbb{R}_+^n \setminus \{(1, 1, \dots, 1)\}$. The ALEM is defined as the pullback metric from the Euclidean space $\mathbb{S}^n$ using a generalized matrix logarithm $\text{mlog}(\cdot)$ [8]:
where $S = U \Sigma U^T$ is the eigendecomposition of S, and $\log_\alpha(\Sigma) = \text{diag}(\log_{a_1} \sigma_1, \log_{a_2} \sigma_2, \dots, \log_{a_n} \sigma_n)$ is the diagonal logarithm. The inverse mapping $\text{mlog}^{-1}(\cdot)$
where $\alpha(\Sigma) = \text{diag}(a_1^{\sigma_1}, a_2^{\sigma_2}, \dots, a_n^{\sigma_n})$. This allows us to define the Adaptive Log-Euclidean Distance (ALED) between two SPD matrices S_1 and S_2
where $\| \cdot \|_F$ is the Frobenius norm. The ALEM provides a flexible and learnable Riemannian metric that adapts to the data distribution.

The manifold attention module operates on the sequence of SPD matrices $\tilde{X} = [\tilde{x}_1, \tilde{x}_2, \dots, \tilde{x}_m]$. As illustrated in Figure 2(a), the module computes query (q_i), key (k_i), and value (v_i) matrices for each $\tilde{x}_i$ using bilinear mappings
where $W_q, W_k, W_v \in \mathbb{R}^{d_u \times d_c}$ are learnable transformation matrices, and $d_u < d_c$ ensures dimensionality reduction. To ensure that q_i, k_i, v_i remain SPD matrices, W_q, W_k, W_v are constrained to be row-full rank.

The similarity between query q_i and key k_j is computed using the ALEM-based distance: The attention matrix $A = [\alpha_{ij}]_{m \times m}$ is then normalized using the Softmax function.

The output of the attention module is computed as the Log-Euclidean mean of the value matrices $v_1, v_2, \dots, v_m$ weighted by the attention scores. After the manifold attention module, the SPD matrices $v_1', v_2', \dots, v_m'$ are mapped back to Euclidean space using the R2E operation. This involves applying the matrix logarithm $\text{Log}(\cdot)$ followed by a flattening operation. Where U and $\sigma_1, \dots, \sigma_{d_u}$ are the eigenvectors and eigenvalues of v_i', respectively. The flattened vectors are then passed through a fully connected layer and a Softmax classifier for final classification.

The loss function for the model is the cross-entropy loss between the predicted output $\hat{y}$ and the ground truth y. The Riemannian gradient descent method is used to update the parameter on the Stiefel manifold. The Euclidean gradients are projected onto the tangent space of the Stiefel manifold, and the retraction operation ensures that the updated weights remain on the manifold.

Regarding computational overhead, the ALEM introduces a learnable diagonal base vector $\alpha \in \mathbb{R}^n$, adding only $\mathcal{O}(n)$ extra parameters compared to the standard Log-Euclidean Metric. This results in negligible additional computation relative to the overall model, making AMAtt highly efficient for practical deployment.

4. Datasets

We have used two publicly available EEG datasets: the BCI Competition IV 2a Dataset (BCIC-IV-2a) [13] for time-asynchronous motor imagery (MI) EEG decoding and the MAMEM EEG SSVEP Dataset II (MAMEM-SSVEP-II) for time-synchronous steady-state visually evoked potential (SSVEP) EEG decoding. Below, we provide detailed descriptions of these datasets and their preprocessing steps.

4.1. BCI Competition IV 2a Dataset (BCIC-IV-2a)

The BCIC-IV-2a dataset is one of the most widely used public EEG datasets, released for the BCI Competition IV in 2008 [13]. It contains EEG recordings from nine subjects performing a four-class motor imagery task. Each subject participated in two sessions on different days. During the task, subjects were instructed to imagine one of four movements (right hand, left hand, feet, and tongue) for four seconds after an instructional cue. Each session consists of 288 trials, with 72 trials for each type of motor imagery.

The EEG signals were recorded using 22 Ag/AgCl electrodes placed at central and surrounding regions, with a sampling rate of 250 Hz. The preprocessing steps for this dataset include:

1) *Down-sampling*: The signals were down-sampled from 256 Hz to 128 Hz.
2) *Band-pass filtering*: A band-pass filter was applied in the range of 4-38 Hz to remove noise and artifacts.
3) *Segmentation*: EEG signals were segmented from 0.5 to 4 seconds (438 timepoints) after the onset of the cue for each trial.

4.2. MAMEM EEG SSVEP Dataset II (MAMEM-SSVEP-II)

The MAMEM-SSVEP-II dataset was used as the representative dataset for time-synchronous EEG data. It consists of EEG recordings from 11 subjects performing an SSVEP-based task. Subjects were instructed to gaze at one of five visual stimuli flickering at different frequencies (6.66, 7.50, 8.57, 10.00, and 12.00 Hz) for five seconds. Each subject executed five runs of five cue-based trials for each stimulation frequency.

The EEG signals were acquired using the EGI 300 Geodesic EEG System (GES 300) equipped with 256 channels at a sampling rate of 250 Hz. The dataset contains five sessions. For evaluation, we assigned the early blocks (sessions 1, 2, and 3) as the training set, session 4 as the validation set, and session 5 as the test set. The preprocessing steps for this dataset include:

1) *Band-pass filtering*: A band-pass filter was applied in the range of 1-50 Hz to remove noise and artifacts.
2) *Channel selection*: Eight channels (PO7, PO3, PO, PO4, PO8, O1, Oz, and O2) in the occipital area (location of the visual cortex) were selected.
3) *Segmentation*: Each trial was segmented into four 1-second segments (1-5 seconds after the onset of the cue), yielding 500 trials of 1-second 8-channel SSVEP signals per subject.

5. Results

In this section, we present the experimental setup, training process, and results of the proposed AMAtt and MAtt models on the BCIC-IV-2a and MAMEM-SSVEP-II datasets. We compare the performance of both models and analyze their training dynamics using accuracy plots.

5.1. Experimental Setup

The experiments were conducted using PyTorch on a GPU-enabled machine. The models were trained using the Adam optimizer, and the best-performing model checkpoints were saved based on validation accuracy. The training process was repeated for multiple subjects to ensure robustness.

The hyperparameters were selected based on a combination of grid search and the settings reported in the original MAtt paper [1]. Specifically, a learning rate of 1×10^{-4} and weight decay of 1×10^{-2} were found to yield stable convergence on the BCIC-IV-2a dataset, while a slightly higher learning rate of 1×10^{-3} was used for MAMEM-SSVEP-II to account for the different signal characteristics. Batch sizes of 128 and 64 were chosen to balance memory efficiency and gradient stability for each dataset respectively.

5.2. Results on BCIC-IV-2a Dataset

The AMAtt and MAtt models were evaluated on the BCIC-IV-2a dataset for motor imagery EEG decoding. The results are summarized below:

1) *AMAtt*: Achieved a test accuracy of *63.19%* at iteration 500. The training accuracy reached *82.54%*.
2) *MAtt*: Achieved a test accuracy of *57.64%* at iteration 500. The training accuracy reached *79.37%*.

The training accuracy plots demonstrate that AMAtt consistently outperforms MAtt in terms of training accuracy and generalization to the validation set. Also AMAtt achieved superior performance with an AUC score of 0.8286 compared to MAtt's 0.7994 AUC. The higher AUC values confirm AMAtt's better discriminative capability between classes.

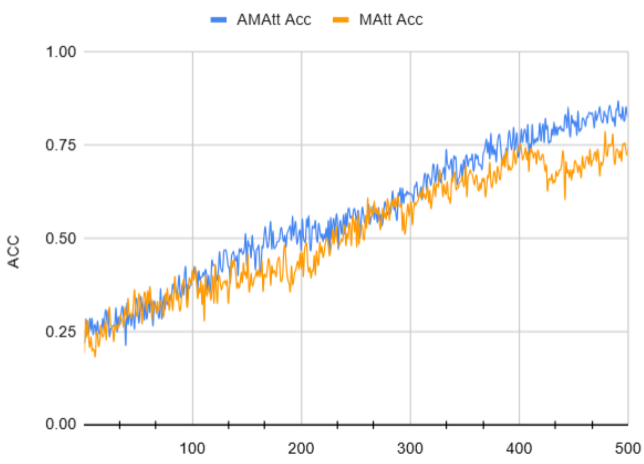

Figure 4. *Training accuracy plots for AMAtt and MAtt on the BCIC-IV-2a dataset.*

5.3. Results on MAMEM-SSVEP-II Dataset

The AMAtt and MAtt models were also evaluated on the MAMEM-SSVEP-II dataset for SSVEP EEG decoding. The results are summarized below:

1) *AMAtt*: Achieved a test accuracy of *46.00%* at iteration 500. The training accuracy reached *77.00%*.
2) *MAtt*: Achieved a test accuracy of *41.40%* at iteration 500. The training accuracy reached *75.33%*.

The training accuracy plots indicate that AMAtt achieves higher training accuracy compared to MAtt, although both models exhibit similar validation performance. AMAtt maintained its advantage with an AUC of 0.6219 outperforming MAtt's 0.6077 AUC score.

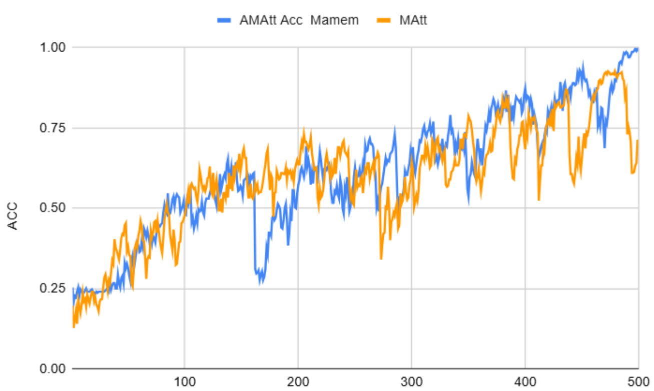

Figure 5. *Training accuracy plots for AMAtt and MAtt on the MAMEM-SSVEP-II dataset.*

6. Conclusion

In this study, we introduced *AMAtt*, an adaptive variant of the *MAtt* architecture, designed to enhance EEG signal decoding by leveraging Riemannian geometry and adaptive mechanisms. The model was rigorously evaluated on two widely used datasets—*BCIC-IV-2a* (motor imagery) and *MAMEM-SSVEP-II* (SSVEP)—demonstrating consistent improvements over the baseline *MAtt* model. On the *BCIC-IV-2a* dataset, *AMAtt* achieved a test accuracy of *63.19%*, significantly outperforming *MAtt*'s *57.64%*. Similarly, on the *MAMEM-SSVEP-II* dataset, *AMAtt* attained a test accuracy of *46.00%*, compared to *MAtt*'s *41.40%*. The training dynamics further confirmed that *AMAtt* not only learns more efficiently but also generalizes better to unseen data, indicating robust adaptation to varying EEG signal characteristics.

The superior performance of *AMAtt* can be attributed to its adaptive mechanisms, which dynamically refine the Riemannian geometric framework to better capture the intrinsic structure of EEG signals. This adaptability proves particularly advantageous in handling both *time-asynchronous* (e.g., motor imagery) and *time-synchronous* (e.g., SSVEP) tasks, where traditional fixed-geometry approaches may struggle. These findings underscore the importance of *adaptive Riemannian geometry* in EEG decoding, suggesting that *learnable transformations* (such as those in *AMAtt*) can significantly enhance model flexibility and discriminative power.

Future work includes extending the evaluation of *AMAtt* to additional EEG datasets, such as those involving motor imagery, emotion recognition, or brain-computer interface applications. Hyperparameter optimization: Investigate the impact of hyperparameters, such as learning rate, batch size, and the number of epochs, on the performance of *AMAtt*. Integration with deep learning architectures: Explore the integration of *AMAtt* with advanced deep learning models, such as transformers or graph neural networks, to further improve EEG decoding performance. Real-time applications: Develop real-time implementations of *AMAtt* for practical brain-computer interface applications, ensuring low latency and high accuracy. Interpretability: Enhance the interpretability of the model by analyzing the learned Riemannian metrics and their relationship to the underlying EEG signal characteristics. These future directions aim to further advance the state-of-the-art in EEG signal decoding and contribute to the development of more robust and efficient brain-computer interface systems.

ORCID

0000-0002-4119-0045
(Syed Mohamed Syed Abubakar Shaihan)

Abbreviations

AIM	Affine-Invariant Metric
ALEM	Adaptive Log-Euclidean Metric
ALED	Adaptive Log-Euclidean Distance
AUC	Area Under the Curve

BCI	Brain-Computer Interface
BCIC-IV-2a	BCI Competition IV 2a Dataset
CNN	Convolutional Neural Network
DL	Deep Learning
EEG	Electroencephalography
E2R	Euclidean to Riemannian
GDL	Geometric Deep Learning
GL	Geometric Learning
LEM	Log-Euclidean Metric
MAMEM-SSVEP-II	MAMEM EEG SSVEP Dataset II
MAtt	Manifold Attention Network
MDM	Minimum Distance to Mean
MI	Motor Imagery
R2E	Riemannian to Euclidean
RG	Riemannian Geometry
SCM	Sample Covariance Matrix
SNR	Signal-to-Noise Ratio
SPD	Symmetric Positive Definite
SSVEP	Steady-State Visual Evoked Potential
TSLDA	Tangent Space Linear Discriminant Analysis

Acknowledgments

The author thanks the creators and maintainers of the BCIC-IV-2a and MAMEM-SSVEP-II datasets for making them publicly available, which enabled the experimental validation of this work, and Prof. Christian Napoli who advised the author throughout this work. This research received no external funding.

Author Contributions

Syed Mohamed Syed Abubakar Shaihan: Conceptualization, Data curation, Formal Analysis, Investigation, Methodology, Project administration, Resources, Software, Supervision, Validation, Visualization, Writing – original draft, Writing – review & editing

Conflicts of Interest

The author declares no conflicts of interest.

References

[1] Pan, Y.-T.; Chou, J.-L.; Wei, C.-S. MAtt: A Manifold Attention Network for EEG Decoding. *Advances in Neural Information Processing Systems 2022*, *35*, pp. 31116–31129. https://doi.org/10.48550/arXiv.2210.01986

[2] Iturrate, I.; Antelis, J.; Minguez, J. Synchronous EEG brain-actuated wheelchair with automated navigation. In Proceedings of the 2009 IEEE International Conference on Robotics and Automation, 2009. https://doi.org/10.1109/ROBOT.2009.5152580

[3] Subha, D. P.; Joseph, P. K.; Acharya U, R.; Lim, C. M. EEG signal analysis: a survey. *Journal of Medical Systems 2010*, *34*(2). https://doi.org/10.1007/s10916-008-9231-z

[4] Al-Qaysi, Z. T.; Zaidan, B. B.; Zaidan, A. A.; Suzani, M. S. A review of disability EEG based wheelchair control system: Coherent taxonomy, open challenges and recommendations. *Computer Methods and Programs in Biomedicine 2018*, *164*. https://doi.org/10.1016/j.cmpb.2018.06.012

[5] Chen, X.; Wang, Y.; Nakanishi, M.; Gao, X.; Jung, T.-P.; Gao, S. High-speed spelling with a noninvasive brain–computer interface. *Proceedings of the National Academy of Sciences 2015*, *112*(44). https://doi.org/10.1073/pnas.1508080112

[6] Barachant, A.; Bonnet, S.; Congedo, M.; Jutten, C. Multiclass brain–computer interface classification by Riemannian geometry. *IEEE Transactions on Biomedical Engineering 2012*, *59*(4), pp. 920–928. https://doi.org/10.1109/TBME.2011.2172210

[7] Monti, F.; Boscaini, D.; Masci, J.; Rodola, E.; Svoboda, J.; Bronstein, M. M. Geometric deep learning on graphs and manifolds using mixture model CNNs. In Proceedings of the IEEE Conference on Computer Vision and Pattern Recognition, 2017. https://doi.org/10.48550/arXiv.1611.08402

[8] Chen, Z.; Song, Y.; Xu, T.; Huang, Z.; Wu, X.-J.; Sebe, N. Adaptive Log-Euclidean Metrics for SPD Matrix Learning. *IEEE Transactions on Image Processing 2024*, *33*, pp. 5194–5205. https://doi.org/10.1109/TIP.2024.3451930

[9] Arsigny, V.; Fillard, P.; Pennec, X.; Ayache, N. Log-Euclidean metrics for fast and simple calculus on diffusion tensors. *Magnetic Resonance in Medicine 2006*, *56*(2), pp. 411–421. https://doi.org/10.1002/mrm.20965

[10] Barbaresco, F. Innovative tools for radar signal processing based on Cartan's geometry of SPD matrices & information geometry. In Proceedings of the 2008 IEEE Radar Conference, 2008. https://doi.org/10.1109/RADAR.2008.4720937

[11] Arsigny, V.; Fillard, P.; Pennec, X.; Ayache, N. Geometric means in a novel vector space structure on symmetric positive-definite matrices. *SIAM Journal on Matrix Analysis and Applications 2007*, *29*(1), pp. 328–347. https://doi.org/10.1137/050637996

[12] Nguyen, X. S. A Gyrovector space approach for symmetric positive semi-definite matrix learning. In Proceedings of the European Conference on Computer Vision, 2022; pp. 52–68. https://doi.org/10.1007/978-3-031-19812-0_4

[13] Brunner, C.; Leeb, R.; Müller-Putz, G.; Schlögl, A.; Pfurtscheller, G. BCI Competition 2008–Graz data set A. *Institute for Knowledge Discovery (Laboratory of Brain-Computer Interfaces), Graz University of Technology 2008*, *16*.

[14] Dimitriadis, S. I. SCZ: A Riemannian schizophrenia diagnosis framework based on the multiplexity of EEG-based dynamic functional connectivity patterns. *Computers in Biology and Medicine 2024*, *180*. https://doi.org/10.1016/j.compbiomed.2024.108862

[15] Lawhern, V. J.; Solon, A. J.; Waytowich, N. R.; Gordon, S. M.; Hung, C. P.; Lance, B. J. EEGNet: A compact convolutional neural network for EEG-based brain–computer interfaces. *Journal of Neural Engineering 2018*, *15*(5), 056013. https://doi.org/10.1088/1741-2552/aace8c

[16] Schirrmeister, R. T.; Springenberg, J. T.; Fiederer, L. D. J.; Glasstetter, M.; Eggensperger, K.; Tangermann, M.; Hutter, F.; Burgard, W.; Ball, T. Deep learning with convolutional neural networks for EEG decoding and visualization. *Human Brain Mapping 2017*, *38*(11), pp. 5391–5420. https://doi.org/10.1002/hbm.23730